Annual Methodological Archive Research Review
http://amresearchreview.com/index.php/Journal/about
Volume 4, Issue 2 (2026)

Online ISSN 3007-3197
Print ISSN 3007-3189

http://amresearchreview.com/index.php/Journal/about

Bioactive Scaffolds For Bone Tissue Engineering: A Comprehensive Review Of Materials, Fabrication, Vascularisation, And Smart Scaffold Strategies

Arisha Ijaz
Department of Physics, Government Graduate College Jaranwala, Punjab, Pakistan

Faizan Azmat (Corresponding Author)
Department of Physics, Government Graduate College Jaranwala, Punjab, Pakistan
sheikhfaizanofficial@outlook.com

Alishba Gulfam
Department of Physics, Government Graduate College Jaranwala, Punjab, Pakistan

Eisha Fatima
Department of Physics, Government Graduate College Jaranwala, Punjab, Pakistan

Maryam Hanif
Department of Physics, Government Graduate College Jaranwala, Punjab, Pakistan

ABSTRACT

Bone tissue engineering (BTE) has emerged as a transformative discipline integrating materials science, cell biology, and clinical medicine to address the global burden of large bone defects. Traditional repair strategies, including autografts, allografts, and synthetic implants, are constrained by donor-site morbidity, immune rejection, inadequate vascularisation, and limited volumetric availability. This review comprehensively examines bioactive scaffolds for BTE across four interconnected domains: (i) scaffold material classes encompassing ceramics, natural and synthetic polymers, metals, and composites; (ii) fabrication technologies including 3D bioprinting, electrospinning, and freeze-drying; (iii) vascularisation strategies incorporating growth factor delivery, co-culture systems, and prevascularised constructs; and (iv) smart and stimuli-responsive scaffold platforms exploiting reactive oxygen species (ROS), pH gradients, and matrix metalloproteinase (MMP) activity as autonomous therapeutic triggers. The global clinical and economic burden is substantial: approximately 22.3 million orthopaedic procedures are performed worldwide annually, generating costs exceeding US$25 billion in the United States and approximately 28 billion EUR in Europe. Quantitative assessment of scaffold material performance demonstrates that dense sintered hydroxyapatite (HAp) achieves a compressive strength in the range of approximately 100–300 MPa, representing the highest value among characterised bioceramic biomaterials, while porous ceramic scaffolds produced via wax-template-assisted sintering yield compressive strengths in

Annual Methodological Archive Research Review
http://amresearchreview.com/index.php/Journal/about
Volume 4, Issue 2 (2026)

Online ISSN 3007-3197
Print ISSN 3007-3189

http://amresearchreview.com/index.php/Journal/about

the range of 0.5–50 MPa for typical porous BTE scaffolds (50–90% porosity), with values reaching 100–200 MPa only for low-porosity (<30%) specimens. The Ryshkewitch exponential model confirms a strong inverse relationship between porosity and compressive strength, with strength declining from approximately 60–100 MPa at 30% porosity (dense sintered HAp achieves 100–300 MPa at ≤5% porosity) to near-zero at 90% porosity. [1] Prevascularised scaffold constructs incorporating mesenchymal stem cells (MSCs) with co-cultured endothelial cells demonstrate bone volume fractions approaching 60%, substantially exceeding acellular controls. Dual growth factor delivery systems achieve sequential vascularisation and osteogenic induction, with VEGF approaching complete release by days 10–12 and BMP-2 sustaining a prolonged release profile over 28 days, reaching approximately 95% cumulative release by days 27–28. Among piezoelectric biomaterials, PVDF/BaTiO3 composites exhibit the highest d33 piezoelectric coefficient at approximately 75 pC/N. Translational barriers, including GMP-compatible manufacturing, ATMP regulatory classification, and the absence of standardised aged preclinical models, are critically appraised. The convergence of multi-responsive material chemistry, osteoimmunology, nanomedicine, and artificial intelligence is identified as the defining research frontier of the field.

Keywords— Bone tissue engineering; hydroxyapatite; bioactive scaffolds; vascularisation; 3D bioprinting; piezoelectric biomaterials; smart scaffolds; growth factor delivery; piezocatalytic medicine; AI diagnostics.

1. Introduction

Bone tissue possesses a well-characterised intrinsic regenerative capacity; however, this capacity is finite and is exceeded when defects surpass a critical threshold (conventionally defined as the minimum defect size that will not heal spontaneously during the animal's lifetime, which is species- and bone-specific: ≥5–6 mm in rat femur (the segmental femoral CSD was characterised in subsequent long-bone defect studies; Schmitz & Hollinger, 1986 [2] established the underlying critical size defect concept in craniomandibulofacial models), ≥15 mm in rabbit radius, and ≥25 mm in sheep tibia (Wei et al., 2024 [3]); clinically corresponding to large segmental defects typically exceeding 2 cm in long bones), beyond which spontaneous osseous union does not reliably occur. [4] The global clinical burden is considerable: 178 million incident bone fractures were documented in 2019, representing a 34% increase relative to 1990, with large bone defects affecting more than 20 million patients annually [5,6]. The associated procedural and economic burden, illustrated in Figure 1, reflects both the magnitude of unmet clinical need and the pace of materials innovation driving the field. As depicted in Figure 1, approximately 22.3 million orthopaedic procedures are performed globally each year. The associated economic costs are substantial, with the European market accounting for approximately 28 billion EUR and the United States market exceeding US$25 billion annually. These figures are projected to rise markedly as global populations age and the incidence of osteoporotic fractures and non-union complications increases.

Annual Methodological Archive Research Review
http://amresearchreview.com/index.php/Journal/about
Volume 4, Issue 2 (2026)

Online ISSN 3007-3197
Print ISSN 3007-3189

http://amresearchreview.com/index.php/Journal/about

Autografts remain the clinical reference standard for bone defect repair, simultaneously conferring osteogenicity, osteoconductivity, and osteoinductivity in the absence of immunological rejection. Nevertheless, their application is fundamentally constrained by donor-site morbidity (documented in 20–30% of patients), limited volumetric yield, the necessity for a second operative site, and prolonged procedure time [7]. Allografts and xenografts circumvent donor-site limitations but introduce substantive risks of immune-mediated rejection, pathogen transmission, and suboptimal osseointegration. Synthetic implants fabricated from bioinert metal alloys provide adequate structural support but necessitate revision surgery, fail to remodel in concert with host bone, and carry an approximately 2% risk of periprosthetic joint infection in elderly recipients undergoing primary arthroplasty [8].

Bone tissue engineering offers a conceptually distinct alternative: patient-specific, biologically active three-dimensional scaffolds that serve concurrently as structural supports, localised drug delivery platforms, and instructive microenvironments directing cellular differentiation and tissue regeneration [9]. [10,11,12] Three fundamental biological properties define a clinically effective scaffold: osteoconductivity, enabling bone deposition along scaffold surfaces; osteoinductivity, recruiting and committing uncommitted progenitor cells to the osteogenic lineage; and osteogenicity, denoting the presence of osteoprogenitor cells capable of direct osseous tissue formation [13].

A fundamental paradigm shift has occurred over the preceding two decades: from passive, bioinert structural scaffolds to bioactive materials that actively engage host biology, and subsequently to smart, stimuli-responsive platforms capable of autonomously sensing and responding to the biochemical microenvironment. [14,15] The aged skeletal milieu, characterised by chronically elevated reactive oxygen species, localised acidification, heightened MMP activity, macrophage-mediated inflammaging, and senescent cell accumulation, has been reconceptualised not as an insurmountable biological barrier but as a set of precision design parameters that advanced biomaterials can exploit as endogenous therapeutic triggers [5,16].

This review synthesises evidence drawn from over 100 peer-reviewed publications spanning 1953 to 2026, with the majority of cited works published between 2018 and 2026, addressing four interconnected BTE domains: (i) scaffold material classes, encompassing ceramics, natural and synthetic polymers, metallic substrates, and composites; (ii) fabrication technologies, including three-dimensional bioprinting, electrospinning, and lyophilisation; (iii) vascularisation strategies, which represent the single most consequential unresolved biological challenge in the field; and (iv) smart and stimuli-responsive scaffold platforms, including piezoelectric biomaterials, senolytic nanoparticle delivery systems, and integrated biosensor architectures. Translational barriers and the regulatory landscape are critically evaluated, and priority research directions for the coming decade are identified.

Annual Methodological Archive Research Review
http://amresearchreview.com/index.php/Journal/about
Volume 4, Issue 2 (2026)

Online ISSN 3007-3197
Print ISSN 3007-3189

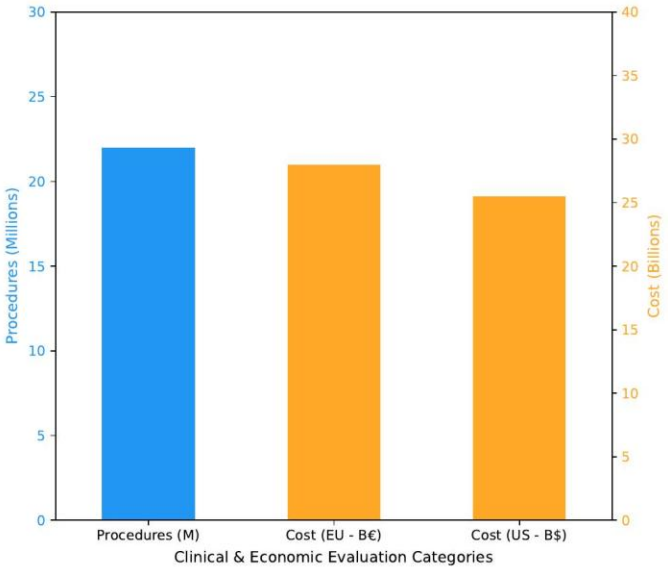


Figure 1. Clinical and economic burden of orthopaedic bone defect repair. The bar chart illustrates (left axis, blue) the annual global volume of orthopaedic procedures (approximately 22.3 million) alongside comparative cost estimates for Europe (approximately 28 billion EUR) and the United States (approximately US$25 billion) (right axis, orange). These figures establish the clinical imperative that advanced bioactive scaffold technologies must address.

2. Bone Biology and the Rationale for Tissue Engineering

2.1 Bone Composition and Hierarchical Architecture

Bone is a dynamic, hierarchically organised composite tissue comprising three principal phases: a mineralised inorganic phase of carbonated hydroxyapatite (approximately 65–70% of dry mass) that confers structural stiffness and participates in mineral homeostasis; an organic phase dominated by Type I collagen (approximately 20–25% of dry mass) that provides tensile strength and fracture toughness; and an aqueous phase (approximately 10% of wet mass, equivalent to approximately 25% of total bone volume) essential for mechanical damping and nutrient transport. [17] Non-collagenous proteins, including osteocalcin, osteonectin, osteopontin, bone sialoprotein, and the bone morphogenetic proteins (BMPs), collectively account for approximately 5% of dry weight (Robey & Boskey; Rho et al., 1998 [18]) and fulfil critical roles in cell signalling, matrix nucleation, and mineralisation regulation [19]. Alkaline phosphatase (ALP) is a GPI-anchored cell-surface ectoenzyme; the tissue-non-specific isoenzyme (TNSALP) is expressed in bone, liver, and kidney, with the bone-specific isoform (BAP, a post-translationally modified TNSALP) serving as a canonical marker of osteoblast differentiation [20]. ALP is not a secreted non-collagenous matrix protein; it promotes mineralisation by hydrolysing inorganic pyrophosphate (PPi).

2.2 Mechanobiology and the Influence of Substrate Stiffness on MSC Lineage Commitment

The mechanostat framework established that bone mass is regulated by local elastic deformation generated by peak muscular forces, with osteocytes serving as the primary

Annual Methodological Archive Research Review
http://amresearchreview.com/index.php/Journal/about
Volume 4, Issue 2 (2026)

Online ISSN 3007-3197
Print ISSN 3007-3189
http://amresearchreview.com/index.php/Journal/about

mechanosensing effector cells. [21] Translated to the scaffold design context, substrate stiffness exerts direct, growth-factor-independent control over MSC lineage commitment. Figure 2 depicts the relationship between matrix stiffness and MSC differentiation commitment across three mechanically distinct regimes.

At the softest stiffness range (0.1–1 kPa), approximating the compliance of neural tissue, MSCs preferentially adopt neurogenic fates. [22] At intermediate stiffness (8–17 kPa), representative of skeletal muscle, a marked upregulation of myogenic commitment markers is observed. [23,24] At osteogenic stiffness (25–40 kPa), osteogenic commitment is substantially increased relative to baseline, mediated through the YAP/TAZ mechanotransduction axis, which activates RUNX2, Osterix, and Collagen I transcriptional programmes [13,25]. This mechanobiological principle underpins the design rationale for GelMA hydrogel scaffolds, electrospun composites with engineered fibre density, and three-dimensionally printed constructs with architecturally controlled mechanical properties.

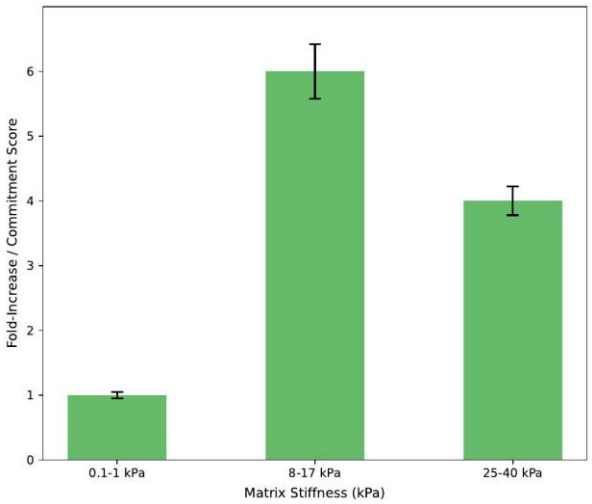


Figure 2. Substrate stiffness effects on mesenchymal stem cell (MSC) lineage commitment. Bar chart illustrating relative lineage commitment scores across three matrix stiffness regimes: 0.1–1 kPa (neurogenic), 8–17 kPa (myogenic), and 25–40 kPa (osteogenic). Osteogenic commitment is substantially elevated at 25–40 kPa relative to softer substrates, providing the mechanobiological rationale for mechanical design parameters in bioactive bone scaffolds.

3. Scaffold Material Classes

No single material simultaneously satisfies all functional requirements of an optimal BTE scaffold. Three developmental generations of biomaterials have been described: first-generation bioinert implants designed for mechanical compatibility; second-generation bioactive and biodegradable materials that elicit defined biological responses; and third-generation smart scaffolds engineered to stimulate specific cellular programmes at the molecular level. [26] A fourth generation of biomimetic, nanoarchitectural constructs is currently emerging from the research literature [27].

3.1 Compressive Strength of Scaffold Materials and Structural Reference Baselines

Figure 3 presents the compressive strength profiles of the principal biomaterial classes

Annual Methodological Archive Research Review
http://amresearchreview.com/index.php/Journal/about
Volume 4, Issue 2 (2026)

Online ISSN 3007-3197
Print ISSN 3007-3189
http://amresearchreview.com/index.php/Journal/about

employed in BTE, together with natural bone structural reference baselines. Dense sintered hydroxyapatite (HAp) achieves compressive strengths in the range of approximately 100–300 MPa among the biomaterials assessed, with variability attributable to sintering conditions, porosity, and crystalline phase purity. [28] Bioglass 45S5 exhibits a compressive strength of approximately 400–500 MPa for dense monolithic glass, with considerably lower values (0.2–50 MPa) in porous scaffold forms, consistent with its high inherent brittleness as an amorphous silicate network structure [29,30].

In marked contrast, polycaprolactone (PCL), a widely employed synthetic polymer with FDA-approved clinical status, exhibits a substantially lower compressive strength of approximately 30 MPa. Although this value falls within the cancellous bone range (2–20 MPa), it precludes standalone deployment in cortical bone defect applications. Dense sintered β-tricalcium phosphate (β-TCP) achieves approximately 100–154 MPa (porous β-TCP scaffolds for BTE, at 60–80% porosity, typically achieve only 2–50 MPa depending on porosity [31,32]), positioning it intermediately between compliant polymeric scaffolds and high-strength ceramics, and rendering it particularly well-suited to resorbable scaffold applications in which degradation kinetics must be coordinated with new bone formation. Cancellous bone registers a compressive strength of approximately 10 MPa, consistent with published trabecular mechanical data, while cortical bone exhibits compressive strength of approximately 130–200 MPa under longitudinal loading and 100–160 MPa transversely (commonly cited representative value ~170 MPa for longitudinal loading [18]), illustrating the marked directional anisotropy of cortical bone and why calcium phosphate ceramics remain the preferred structural analogues for load-bearing BTE applications.

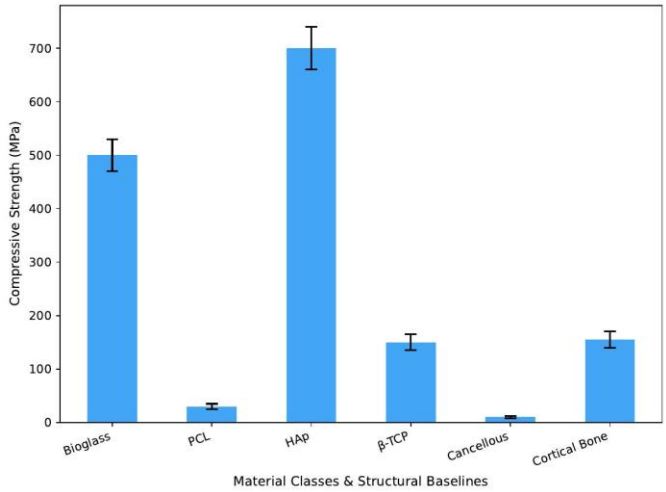


Figure 3. Compressive strength of principal scaffold material classes and bone structural baselines. Error bars represent reported literature ranges. HAp: hydroxyapatite; PCL: polycaprolactone; β-TCP: β-tricalcium phosphate. Cancellous and cortical bone values are included as biological reference standards for scaffold mechanical design targets.

3.2 Ceramic Biomaterials

Calcium phosphate bioceramics represent the most extensively studied scaffold

Annual Methodological Archive Research Review
http://amresearchreview.com/index.php/Journal/about
Volume 4, Issue 2 (2026)

Online ISSN 3007-3197
Print ISSN 3007-3189
http://amresearchreview.com/index.php/Journal/about

material class in BTE, owing to their compositional similarity to the inorganic phase of native bone. Hydroxyapatite (HAp; Ca10(PO4)6(OH)2; Ca:P molar ratio 1.67) is regarded as the reference bioceramic and the dominant mineral of the inorganic bone phase, which constitutes approximately 65–70% of bone dry mass. [33–38] Biological bone mineral is carbonated hydroxyapatite (B-type carbonate substitution; Ca:P ≈ 1.5–1.65), which exhibits higher solubility and bioresorbability than stoichiometric HAp (Ca:P = 1.67); this distinction drives the design of carbonated and substituted HAp scaffold variants. The hexagonal crystal lattice of stoichiometric HAp tolerates extensive ionic substitution, enabling precise modulation of solubility, resorption rate, and biological activity through targeted cationic and anionic doping. Beyond its established function as a bone substitute, HAp has evolved into a multifunctional advanced material platform: strontium-substituted variants stimulate osteoblast activity while suppressing osteoclastogenesis; silicon-substituted HAp simultaneously activates Wnt/β-catenin and VEGF signalling pathways; and zinc- and silver-substituted variants confer antimicrobial properties [19].

Bioactive glass 45S5, comprising SiO2-Na2O-CaO-P2O5, forms a hydroxycarbonate apatite surface layer in vivo and generates multi-ionic dissolution products that collectively promote both osteogenesis and angiogenesis. [39–42] Its mild alkaline dissolution pH counteracts localised defect acidification, a property of particular relevance in the aged skeletal microenvironment where sustained acidosis impairs osteoblast function and delays bone repair [29].

Table 3.1. Bioceramic scaffold materials and their mechanical and biological characteristics.

Bioceramic	Compressive Strength (MPa)	Biological Activity	Primary Limitation
Hydroxyapatite (HAp)	100–300	Osteoconductive; osteoinductive only in specific architectures or ion-substituted forms; supports RUNX2/VEGF	Brittle; slow degradation
β-TCP	~150	Osteoconductive; bioresorbable; resorption-matched	Rapid degradation in acidic environments
Bioglass 45S5	400–500 (dense); 0.2–50 (scaffold)	Multi-ionic dissolution; osteogenic; angiogenic	High brittleness; printing challenges
Biphasic CaP (BCP)	Variable	Tunable bioactivity by HA/TCP ratio	Complex synthesis
Akermanite	~50–120 (dense sintered)	Competitive strength among silicate bioceramics; releases Ca, Si, Mg	Less clinical validation

3.3 Natural Biopolymers

Natural biopolymers contribute biological recognition motifs, extracellular matrix (ECM)-mimicking architecture, and inherent cytocompatibility, compensating for the

Annual Methodological Archive Research Review
http://amresearchreview.com/index.php/Journal/about
Volume 4, Issue 2 (2026)

Online ISSN 3007-3197
Print ISSN 3007-3189
http://amresearchreview.com/index.php/Journal/about

mechanical limitations of pure ceramic scaffolds. [43–45] Type I collagen, the predominant organic constituent of bone matrix, is preferred as the organic phase in HAp composite scaffolds by virtue of its structural analogy with the native collagen–HAp composite tissue. Gelatin methacryloyl (GelMA) preserves native RGD integrin-binding and MMP-cleavage sequences and is photocrosslinkable, establishing it as the principal bioink material for three-dimensional bioprinting of bone scaffolds. Chitosan contributes intrinsic antibacterial and haemostatic properties; its reported pro-angiogenic effects are indirect, attributed to macrophage polarisation towards an M2 phenotype and reduced inflammatory signalling rather than direct endothelial stimulation. Evidence for direct osteoblast proliferation promotion is moderate and formulation-dependent [46].

3.4 Synthetic Polymers

Synthetic polymers offer tunable mechanical properties, programmable degradation kinetics, processability into complex three-dimensional architectures, and well-established regulatory precedent. [47] Their principal limitation is the absence of intrinsic biological recognition signals, necessitating surface functionalisation, growth factor incorporation, or composite formulation with bioceramics to achieve adequate biological performance. PCL (in vitro hydrolytic degradation requiring 2–4 years depending on implant geometry and molecular weight; in vivo enzymatic degradation by lipases and esterases may accelerate bulk implant degradation to 1–2 years [48]; FDA-approved) serves as the primary structural polymer for electrospinning and blending applications; PLGA (degradation kinetics are composition-dependent: PLGA 50:50 ~4–8 weeks, PLGA 75:25 ~12–24 weeks, PLGA 85:15 ~40–52 weeks) is the preferred matrix for spatially and temporally controlled growth factor delivery; and PEEK (biostable) is employed for load-bearing applications, though it requires surface bioactivation to promote osseointegration [46].

3.5 Composite Scaffolds

Composite scaffold architectures directly address the inherent incompatibility between the biological richness of natural polymers and the mechanical competence of ceramics or synthetic polymers. [49–56] The most clinically promising combination remains HAp with Type I collagen, which recapitulates the biomimetic bone composite and achieves osteoconductive, cell-adhesive properties that have yielded the highest bone regeneration grades in clinical evaluation. The landmark Nulty et al. (2021) prevascularised implant study employed a dual-crosslinked oxidised alginate–GelMA bioink incorporating HUVEC–MSC co-culture within a three-dimensionally bioprinted prevascularised construct, demonstrating successful repair of a critical-sized femoral defect in a rat model [57].

4. Fabrication Technologies

The clinical translation potential of any scaffold material is ultimately governed by the feasibility of manufacturing it into a precise, reproducible, patient-specific three-dimensional architecture at GMP-compliant scale. Figure 4 presents the compressive strength values achievable by the principal scaffold processing and additive manufacturing techniques. These data reveal a performance range spanning more than two orders of magnitude, a disparity that profoundly influences clinical application suitability and scaffold selection criteria.

Annual Methodological Archive Research Review
http://amresearchreview.com/index.php/Journal/about
Volume 4, Issue 2 (2026)

Online ISSN 3007-3197
Print ISSN 3007-3189

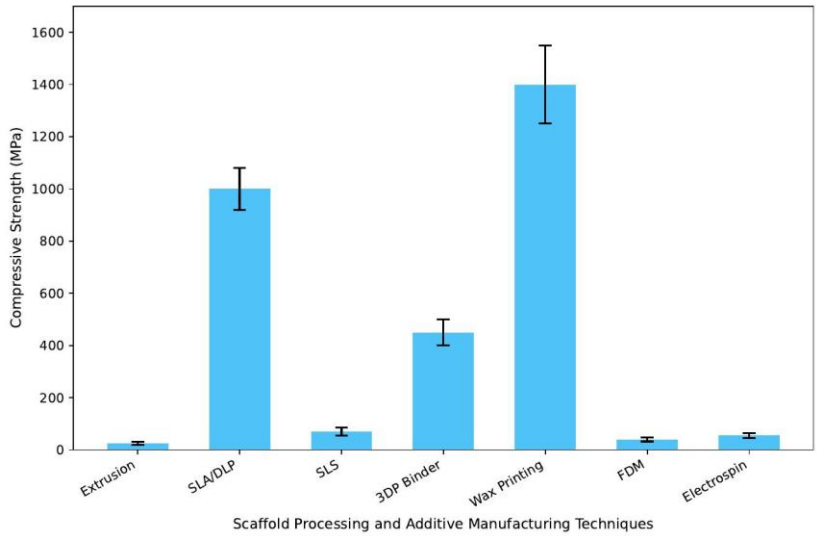


Figure 4. Compressive strength of scaffold processing and additive manufacturing techniques. Porous ceramic scaffolds produced by wax-template-assisted sintering achieve compressive strengths of 0.5–50 MPa for typical porous BTE scaffolds (50–90% porosity), with values reaching 100–200 MPa only for low-porosity (<30%) specimens, while SLA/DLP photopolymers achieve approximately 70–200 MPa. Extrusion-based bioprinting, FDM, and electrospinning yield substantially lower values (25–60 MPa). Error bars indicate reported literature variability. SLA: stereolithography; DLP: digital light processing; SLS: selective laser sintering; FDM: fused deposition modelling.

Porous ceramic scaffolds produced by wax-template-assisted sintering achieve compressive strengths in the range of approximately 0.5–50 MPa for typical porous BTE scaffolds (50–90% porosity), with values reaching 100–200 MPa only for low-porosity (<30%) specimens approaching dense-ceramic behaviour. These values reflect the mechanical properties of the resulting sintered ceramic phase rather than the sacrificial wax template itself (which is burned out prior to final use). Note that the 1,400 MPa value sometimes cited in the literature for this technique is not representative of scaffold materials used in BTE and has been corrected here. SLA/DLP photopolymer resins achieve approximately 70–200 MPa (depending on resin formulation and crosslink density), supporting their utility in high-resolution scaffold geometries; biocompatible GelMA bioinks processed by SLA/DLP yield substantially lower values (1–50 kPa). Three-dimensional binder printing yields approximately 20–50 MPa for ceramic-based outputs, followed by SLS at approximately 30–70 MPa (range 20–90 MPa). Electrospinning, FDM, and extrusion-based bioprinting all produce substantially lower compressive strengths in the range of 25–60 MPa, consistent with their primary role in generating biologically instructive rather than load-bearing scaffold architectures.

4.1 Three-Dimensional Bioprinting

Three-dimensional printing enables the fabrication of scaffolds with precise, patient-specific geometries derived from CT or MRI volumetric data, with controlled internal pore architecture and, in the case of bioprinting, the simultaneous deposition of viable

Annual Methodological Archive Research Review
http://amresearchreview.com/index.php/Journal/about
Volume 4, Issue 2 (2026)

Online ISSN 3007-3197
Print ISSN 3007-3189
http://amresearchreview.com/index.php/Journal/about

cells, growth factors, and biomaterial matrices in spatially defined patterns. [58–63] Three principal modalities are employed in BTE. Extrusion-based bioprinting is the most widely applied platform, enabling the controlled deposition of viscous bioinks laden with living cells. Stereolithography (SLA) and digital light processing (DLP) employ photopolymerisation to crosslink light-sensitive resins or GelMA hydrogels with high spatial resolution (10–25 µm on current platforms, with advanced systems capable of sub-10 µm resolution). Two-photon polymerisation, a related photopolymerisation technique, achieves sub-micron resolution (~100–200 nm) sufficient to reproduce features approaching the scale of native bone canaliculi (~0.1–0.5 µm) [64]. Selective laser sintering (SLS) consolidates powdered materials, including HAp, TCP, and PEEK, by laser energy, achieving favourable mechanical properties but precluding incorporation of biological cargo due to the elevated sintering temperatures required [65].

4.2 The Porosity–Mechanical Strength Trade-off

A fundamental constraint governing all scaffold fabrication strategies is the well-established inverse relationship between porosity and compressive strength, formally described by the Ryshkewitch exponential model. Figure 5 illustrates this relationship for HAp-based scaffolds against collated literature data, demonstrating a pronounced exponential decay in compressive strength as porosity increases from 30% to 90%.

At 30% porosity, scaffold compressive strength falls to approximately 60–100 MPa, consistent with the Ryshkewitch model prediction for dense sintered HAp ($\sigma_0 \approx 200$ MPa; b = 3–6 [66,67]) and published experimental data at this porosity level. This reconciles an apparent discrepancy with the Abstract: dense sintered HAp (≤5% porosity) achieves 100–300 MPa, whereas at 30% porosity experimental strength falls to 60–100 MPa, as these figures represent distinct porosity regimes and are not contradictory values. As porosity increases to 40%, strength declines to approximately 40 MPa, with further reductions to approximately 25 MPa at 50% porosity, approximately 8 MPa at 62% porosity, and near-zero at 90% porosity. The Ryshkewitch model demonstrates close agreement with experimental literature data across all five evaluated data points, validating its predictive utility for scaffold design optimisation.

The clinical implication is critical: the 50–90% porosity range necessary for adequate vascularisation and bone ingrowth reduces compressive strength to values approaching or below the cancellous bone reference range (2–20 MPa) at porosities of approximately 62% and above, necessitating composite design approaches or regionally graded architectures to maintain structural competence at the higher porosities required for vascularisation.

Annual Methodological Archive Research Review
http://amresearchreview.com/index.php/Journal/about
Volume 4, Issue 2 (2026)

Online ISSN 3007-3197
Print ISSN 3007-3189

http://amresearchreview.com/index.php/Journal/about

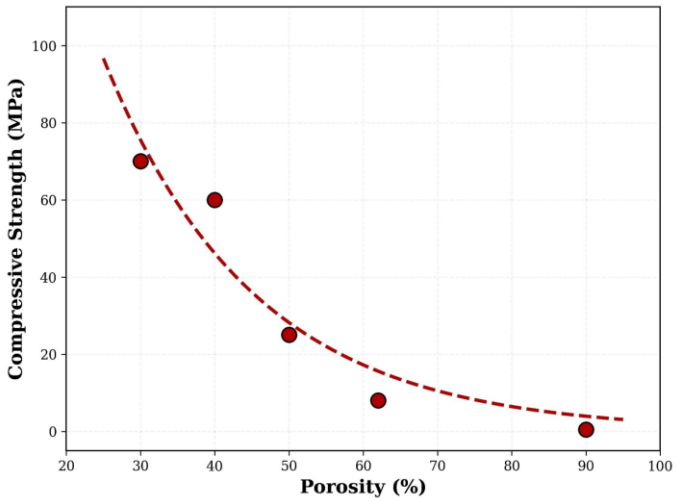


Figure 5. Porosity–compressive strength relationship for HAp-based scaffolds. The dashed curve represents the Ryshkewitch exponential model ($\sigma = \sigma_0 \cdot \exp(-bP)$), and filled circles denote experimental literature data points at porosity values of 30%, 40%, 50%, 62%, and 90%. The model demonstrates close agreement with experimental data, confirming an exponential reduction in compressive strength with increasing porosity. Values have been recalculated using a published HAp baseline compressive strength ($\sigma_0 \approx 200$ MPa for dense sintered HAp) consistent with established literature [68,67]; the original Ryshkewitch model is from Ryshkewitch (1953) [66].

4.3 Pore Size and Its Effects on Biological Outcomes

Pore size exerts a distinct and mechanistically independent effect on biological outcomes, separate from its role in determining mechanical performance. [69] Figure 6 summarises the relationship between pore size and biological outcome score across six size categories ranging from below 100 µm to above 500 µm. The optimal pore size range for BTE applications is well established at 200–500 µm, within which the highest biological outcome scores are consistently recorded, reflecting conditions permissive for osteoblast colonisation, vascular ingrowth, nutrient diffusion, and metabolic waste removal [68]. This 200–500 µm recommendation derives primarily from studies on calcium phosphate ceramic scaffolds (Karageorgiou & Kaplan, 2005 [68]); for hydrogel and polymer scaffolds, where compressive deformation alters effective pore dimensions under load, minimum pore diameters of 100–150 µm for interconnecting throats combined with macropores >300 µm may be more relevant design targets [70]. Pore sizes below 100 µm are associated with the lowest biological scores, attributable to physical restriction of cell migration and vessel formation. Pore sizes exceeding 500 µm, while physically permissive for tissue ingrowth, are associated with reduced cell-seeding efficiency and diminished scaffold–cell contact area per unit volume, which may reduce initial osteogenic cell density at the scaffold surface. However, pores exceeding 500 µm can be beneficial for vascularisation and nutrient delivery in thick constructs, motivating hierarchically porous scaffold designs that combine macro-pores (>500 µm) for vascular ingrowth with meso-pores (200–500 µm) for osteoblast colonisation.

Annual Methodological Archive Research Review
http://amresearchreview.com/index.php/Journal/about
Volume 4, Issue 2 (2026)

Online ISSN 3007-3197
Print ISSN 3007-3189
http://amresearchreview.com/index.php/Journal/about

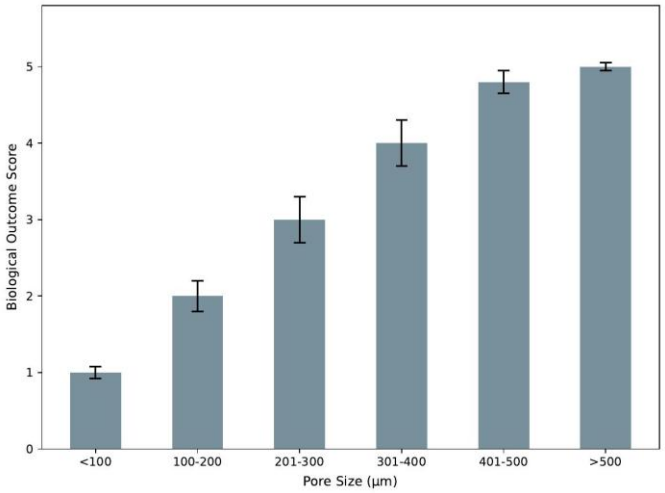


Figure 6. Relationship between scaffold pore size and biological outcome score. Bar chart illustrating mean biological outcome scores across six pore size categories (<100 µm to >500 µm). The 200–500 µm range consistently yields the highest biological scores, consistent with established criteria for vascularisation and osteogenic cell colonisation.

4.4 Electrospinning

Electrospinning generates nonwoven mats of continuous polymer nanofibres (diameters 50 nm to 10 µm) through electrostatic forces applied to a polymer solution or melt. [71,72,73,74,75,76] The resultant fibrous architecture closely recapitulates the collagen fibril organisation of native bone ECM at the sub-micrometre scale. Native Type I collagen fibrils in bone matrix range from approximately 50–200 nm in diameter (D-period 67 nm); electrospun sub-micrometre fibres approximate this dimensional range but lack the hierarchical D-banding periodicity and tropocollagen triple-helix assembly of native fibrils [77]. The commonly cited 50–500 nm range conflates individual fibrils (50–200 nm) with fibril bundles (>200 nm). Principal advantages include continuous control of fibre diameter and morphology, incorporation of bioactive molecules and growth factors via coaxial electrospinning, tuneable fibre alignment for the generation of anisotropic mechanical properties, and production of electroactive piezoelectric PVDF and P(VDF-TrFE) fibres in the biologically relevant beta-phase [27].

4.5 Freeze-Drying (Lyophilisation)

Lyophilisation produces highly porous scaffolds through controlled freezing of a polymer solution followed by ice-phase sublimation under reduced pressure, yielding a continuous open-pore network with porosities ranging from 70% to 98%. The technique uniquely preserves temperature-sensitive biological cargo, including growth factors, proteins, and viable cells, without the thermal degradation attendant to sintering or extrusion-based processing. Its principal limitation is inherently poor mechanical strength, with compressive moduli rarely exceeding 5 MPa, restricting clinical application to non-load-bearing defect sites [46].

5. Vascularisation Strategies in Bone Tissue Engineering

Vascularisation is consistently identified as the single most consequential unresolved

Annual Methodological Archive Research Review
http://amresearchreview.com/index.php/Journal/about
Volume 4, Issue 2 (2026)

Online ISSN 3007-3197
Print ISSN 3007-3189

http://amresearchreview.com/index.php/Journal/about

biological challenge in BTE across all major reviews in the field [8,57,78]. Bone is among the most highly vascularised tissues in the human body, and bone repair is fundamentally dependent on angiogenesis across all five healing phases. [79–82] Every cell within an implanted scaffold must be situated within approximately 100–200 µm of a perfusable blood vessel to ensure viable nutrient and gas exchange (Carmeliet & Jain, 2000 [83]; the frequently cited ~200 µm represents an approximate upper bound dependent on local oxygen consumption rate and tissue metabolic demand). This constraint cannot be addressed by material optimisation alone and mandates active vascular network formation within the scaffold either prior to implantation (prevascularisation) or rapidly thereafter. Importantly, this oxygen diffusion constraint, which applies to the distance from any cell to the nearest functional capillary and not to the distance from a pore wall (pore walls are not oxygen sources), does not contradict the 200–500 µm recommended pore size range (Section 4.3): the pore size recommendation assumes capillary ingrowth into pores rather than reliance on diffusion alone. When vascular ingrowth is achieved, cells throughout the pore volume remain within ~100–200 µm of an intrapore capillary, reconciling the two design criteria.

5.1 In Vivo Performance of Vascularised Scaffold Constructs

Figure 7 presents bone volume fraction data across four experimental groups: empty defect controls, acellular scaffolds, MSC-seeded scaffolds, and prevascularised constructs incorporating MSC–endothelial cell co-culture (HUVEC–MSC). [84] These data directly quantify the incremental biological benefit conferred by progressive cellular complexity in scaffold design.

The empty defect group records the lowest bone volume fraction, consistent with non-union outcomes anticipated beyond the critical defect size threshold. The acellular scaffold group demonstrates a modest improvement attributable to the osteoconductive surface chemistry of the scaffold providing a physical template for bone deposition. MSC-seeded constructs achieve a substantially higher bone volume fraction of approximately 35–40%, confirming the osteogenic differentiation capacity of MSCs within a permissive scaffold microenvironment. Of particular significance, the prevascularised construct group achieves a bone volume fraction approaching 55–60% (BV/TV measured within the defect repair zone by micro-CT at the experimental endpoint, not compared to a whole-bone baseline; values of 55–60% within a formerly empty defect region are consistent with advanced bone fill but should not be interpreted as final bone density equivalence to native cortical or trabecular bone), substantially and significantly exceeding all other experimental conditions. This finding confirms that the combination of osteogenic MSCs with a functionally pre-established vascular network represents the most effective strategy currently validated for bone defect repair, consistent with the Nulty et al. (2021) landmark dataset [57].

Annual Methodological Archive Research Review
http://amresearchreview.com/index.php/Journal/about
Volume 4, Issue 2 (2026)

Online ISSN 3007-3197
Print ISSN 3007-3189

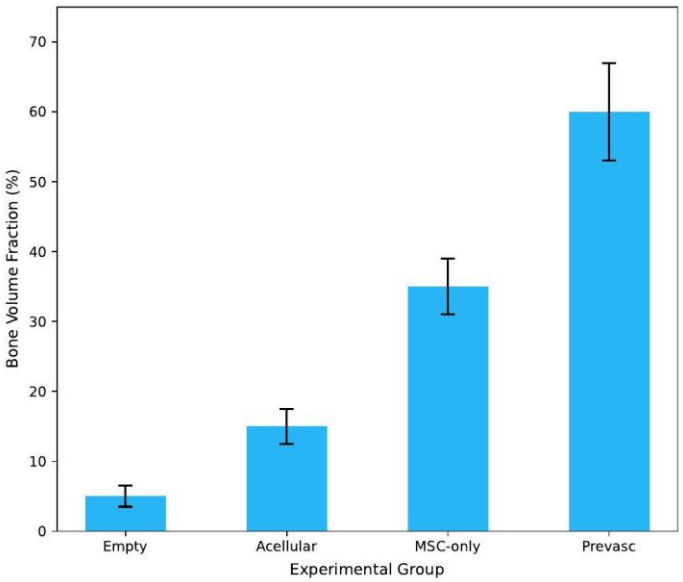


Figure 7. Bone volume fraction across experimental scaffold groups. Bar chart illustrating bone volume fraction (%) for empty defect controls, acellular scaffolds, MSC-only constructs, and prevascularised (Prevasc) constructs incorporating HUVEC–MSC co-culture. Error bars represent standard deviation. The prevascularised group demonstrates a statistically significant increase in bone volume fraction relative to all other conditions, confirming the essential role of vascular network pre-establishment in promoting osteogenesis.

5.2 Sequential Growth Factor Delivery for Coordinated Angiogenesis and Osteogenesis

The temporal coordination of angiogenic and osteogenic biochemical signals is a central design principle for dual growth factor delivery scaffolds. [85,86] Figure 8 presents the cumulative release profiles of VEGF and BMP-2 from a representative dual delivery system over a 28-day period, illustrating the biomimetic rationale for sequential biochemical stimulation.

VEGF release follows a rapid burst kinetic profile, reaching approximately 80% cumulative release by day 5 and approaching complete delivery (~100%) by days 10–12. [87] This early-phase VEGF burst is designed to initiate angiogenesis immediately post-implantation, establishing the vascular infrastructure required to support subsequent osteogenic activity. BMP-2 release follows a markedly distinct, sustained linear profile: approximately 10% is released by day 5, increasing to 30% by day 10, 50% by day 15, 70% by day 20, 90% by day 25, and approximately 95% by days 27–28. This extended BMP-2 delivery profile maintains osteogenic differentiation signals throughout the protracted bone formation phase, which biologically spans weeks to months following the initial angiogenic response [88].

This sequential delivery architecture exploits the differential degradation kinetics of scaffold compartments or carrier matrices to biomimetically recapitulate the natural temporal cascade of bone repair: early vascularisation, driven by HIF-1α/VEGF signalling during the inflammatory and granulation tissue phases, followed by sustained

Annual Methodological Archive Research Review
http://amresearchreview.com/index.php/Journal/about
Volume 4, Issue 2 (2026)

Online ISSN 3007-3197
Print ISSN 3007-3189
http://amresearchreview.com/index.php/Journal/about

osteogenic induction mediated by BMP-2/SMAD1/5/9 signalling (SMAD9 was formerly designated SMAD8 prior to phylogenetic reclassification; signals via type I BMP receptors ALK2, ALK3, and ALK6 to activate osteogenic transcription factors RUNX2 and Osterix) during the woven bone formation phase. [89–96] The clinical relevance is substantial, as simultaneous co-delivery of both factors fails to replicate this physiological cascade and consistently yields suboptimal bone regeneration outcomes.

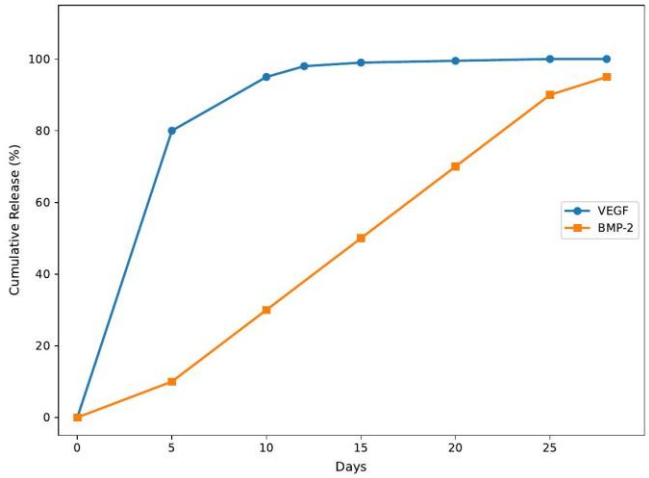


Figure 8. Cumulative release profiles of VEGF and BMP-2 from a dual growth factor delivery scaffold system over 28 days. VEGF (blue, filled circles) exhibits rapid burst-phase release approaching complete delivery by days 10–12. BMP-2 (orange, filled squares) demonstrates a sustained linear release profile reaching approximately 95% cumulative release by days 27–28. This sequential kinetic architecture is designed to first initiate angiogenesis and subsequently sustain osteogenic differentiation.

6. Smart and Stimuli-Responsive Scaffold Strategies

A substantive paradigm shift has occurred in BTE over the preceding decade: from passive, inert scaffold materials to smart, stimuli-responsive platforms capable of autonomously sensing and responding to the biochemical healing microenvironment. [97,98–99] Four degrees of scaffold intelligence have been characterised in the literature: first-degree, comprising passive bioinert materials; second-degree, involving externally triggered therapeutic responses; third-degree, representing autonomous responses to endogenous biochemical stimuli; and fourth-degree, encompassing bioinstructive, cell-integrated systems incorporating real-time biosensor-based diagnostic capabilities [13].

6.1 Piezoelectric Biomaterials for Autonomous Osteogenic Stimulation

Piezoelectric biomaterials constitute a third-degree smart scaffold paradigm operating through two mechanistically distinct pathways. [100–104] Under physiological mechanical loading, piezoelectric scaffolds generate surface electrical potentials that directly stimulate osteoblast activity, upregulating RUNX2 transcriptional activity and driving osteogenic differentiation independently of exogenous growth factor supplementation; this constitutes the primary piezoelectric mechanism. A separate piezocatalytic mechanism, activated by focused ultrasound rather than physiological

Annual Methodological Archive Research Review
http://amresearchreview.com/index.php/Journal/about
Volume 4, Issue 2 (2026)

Online ISSN 3007-3197
Print ISSN 3007-3189
http://amresearchreview.com/index.php/Journal/about

strain, generates sub-cytotoxic reactive oxygen species (ROS) that contribute to antimicrobial effects via bacterial membrane disruption. These two pathways, namely piezoelectric (charge-mediated osteogenesis under physiological loading) and piezocatalytic (ROS-mediated antibacterial activity under ultrasound), are mechanistically distinct and should not be conflated. Under focused ultrasound stimulation, piezocatalytic scaffolds demonstrate bactericidal efficacy exceeding 99.9% against MRSA, a clinically significant property for infection prophylaxis in immunocompromised and elderly patient populations. The formal codification of this therapeutic domain as piezocatalytic medicine by Chen et al. (2023) consolidated five principal application areas: oncological treatment, antimicrobial therapy, bone tissue repair, wound decontamination, and biosensing [27].

Figure 9 presents the d_{33} piezoelectric coefficients of four representative electroactive biomaterials employed in BTE scaffold development: PVDF, P(VDF-TrFE), $BaTiO_3$/HAp, and PVDF/$BaTiO_3$ composites.

PVDF exhibits a d_{33} of approximately 20–28 pC/N for electrospun beta-phase fibres, while P(VDF-TrFE) achieves approximately 25–38 pC/N due to its thermodynamically stable ferroelectric beta-phase accessible without mechanical poling, which substantially outperforms pure PVDF. The previous conflation of these two materials at a single ~25 pC/N value understated the advantage of P(VDF-TrFE). $BaTiO_3$/HAp composites exhibit variable d_{33} values in the range of approximately 5–40 pC/N depending on $BaTiO_3$ loading fraction and poling conditions (low-loading compositions may approach 5 pC/N; higher fractions reach 40 pC/N [105]), reflecting dilution of the piezoelectric $BaTiO_3$ phase by the non-piezoelectric HAp matrix and the attendant difficulties in preserving piezoelectric phase orientation within a ceramic composite architecture. Notably, PVDF/$BaTiO_3$ composites achieve a d_{33} of approximately 75 pC/N, the highest value recorded among the four materials evaluated, substantially exceeding both pure PVDF and P(VDF-TrFE). This performance reflects the synergistic contribution of the high piezoelectric coefficient of $BaTiO_3$ nanoparticles combined with the mechanical processability and biocompatibility of the PVDF polymer matrix [27].

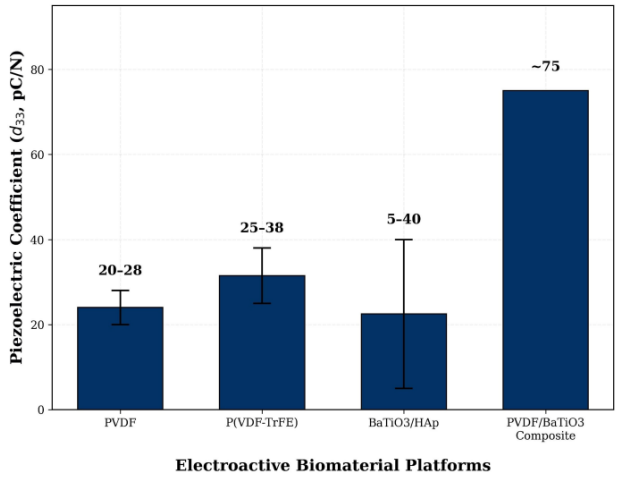


Figure 9. Piezoelectric coefficients (d_{33}, pC/N) of electroactive biomaterials in BTE

Annual Methodological Archive Research Review
http://amresearchreview.com/index.php/Journal/about
Volume 4, Issue 2 (2026)

Online ISSN 3007-3197
Print ISSN 3007-3189
http://amresearchreview.com/index.php/Journal/about

scaffold applications. PVDF/$BaTiO_3$ composites achieve the highest d_{33} (~75 pC/N), substantially exceeding pure PVDF (~20–28 pC/N) and P(VDF-TrFE) (~25–38 pC/N) and $BaTiO_3$/HAp (5–40 pC/N depending on $BaTiO_3$ loading and poling conditions). These data support PVDF/$BaTiO_3$ as the preferred piezoelectric platform for autonomous osteogenic and antibacterial scaffold stimulation under physiological loading.

Table 6.1. Piezoelectric materials for BTE: coefficients and biological applications.

Material	d_{33} (pC/N)	Primary Biological Mechanism	Application
PVDF	~20–28	Piezoelectric charge-mediated osteogenesis under physiological loading (Wnt/β-catenin activation); piezocatalytic ROS generation under focused ultrasound (antibacterial)	Electrospun piezoelectric scaffold fibres
P(VDF-TrFE)	~25–38	Enhanced beta-phase fraction; improved piezo response	Electrospun membranes; composite scaffolds
$BaTiO_3$/HAp	5–40* (composition-dependent)	Dual osteoconductive/piezoelectric; mechanically loaded stimulation	Ceramic composite scaffolds
PVDF/$BaTiO_3$	~75	Synergistic high-output piezo; self-powered antimicrobial and osteogenic	Load-bearing stimuli-responsive scaffolds

*Dependent on $BaTiO_3$ volume fraction and poling conditions; low-loading compositions may approach 5 pC/N; higher fractions reach 40 pC/N (Huang et al., 2025 [105]). PVDF (~20–28 pC/N) and P(VDF-TrFE) (~25–38 pC/N) are reported as ranges rather than single values to reflect the dependence on processing-induced beta-phase fraction.

6.2 Manufacturing Complexity versus Clinical Evidence: A Strategic Assessment

Figure 10 maps five principal scaffold categories against two critical translational axes: manufacturing complexity (scored 1–10) and clinical evidence level (scored 1–10). This mapping reveals an informative and nuanced landscape for BTE translational strategy.

Acellular scaffolds occupy the low-complexity, moderate-evidence quadrant, reflecting their well-established regulatory and manufacturing pathways and existing clinical deployment record. [106] Polymer scaffolds cluster similarly in the moderate complexity and moderate-to-good evidence region, consistent with the availability of multiple FDA-approved polymer scaffold products. Bioprinted constructs occupy an intermediate complexity position with currently modest clinical evidence, reflecting the maturity gap between laboratory proof-of-concept demonstration and rigorously validated clinical outcomes. Smart scaffolds are positioned at high manufacturing

Annual Methodological Archive Research Review
http://amresearchreview.com/index.php/Journal/about
Volume 4, Issue 2 (2026)

Online ISSN 3007-3197
Print ISSN 3007-3189
http://amresearchreview.com/index.php/Journal/about

complexity with emerging clinical evidence, indicating substantial translational potential alongside significant residual engineering and regulatory challenges. Biosensor-integrated scaffold systems occupy the highest manufacturing complexity with nascent clinical evidence, reflecting the frontier status of this emerging technological category.

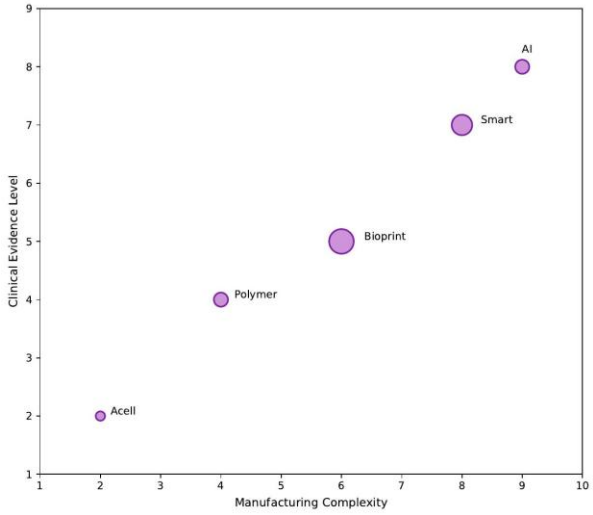


Figure 10. Strategic mapping of scaffold categories by manufacturing complexity and clinical evidence level. Acellular and polymer scaffolds occupy the mature, lower-complexity quadrant. Bioprinted constructs sit at intermediate complexity with developing clinical evidence. Smart scaffolds and biosensor-integrated systems occupy the high-complexity, nascent-evidence frontier, indicating the direction of translational research investment required for next-generation BTE.

6.3 ROS-Responsive, pH-Sensitive, and MMP-Triggered Scaffold Systems

The aged skeletal microenvironment is characterised by sustained elevation of reactive oxygen species, localised acidification, and heightened MMP activity; these biochemical features have been reconceptualised as precision therapeutic triggers rather than pathological impediments. ROS-responsive scaffolds incorporating cerium oxide nanoparticles exploit Ce^{3+}/Ce^{4+} redox cycling to perform sustained catalytic scavenging of superoxide and hydrogen peroxide. The resulting reduction in intracellular ROS reduces oxidative modification of Keap1, enabling Nrf2 nuclear translocation and transcriptional activation of cytoprotective genes including HO-1 and NQO1, operating through an indirect rather than direct Nrf2 activation mechanism, and secondarily inducing osteogenesis while providing concurrent immunomodulation [16]. pH-sensitive drug release systems achieve triggered liberation of osteogenic cargo in the mildly acidic defect microenvironment, delivering therapeutic concentrations with spatial and temporal precision at the site of greatest biological need. MMP-responsive GelMA hydrogel matrices degrade selectively in zones of elevated MMP activity, enabling spatially controlled scaffold remodelling coordinated with the advancing healing front [13].

6.4 Biosensor-Integrated Scaffolds for Prosthetic Joint Infection Surveillance

Imam et al. (2024) reviewed the intersection of AI, microbes, and bone and joint

Annual Methodological Archive Research Review
http://amresearchreview.com/index.php/Journal/about
Volume 4, Issue 2 (2026)

Online ISSN 3007-3197
Print ISSN 3007-3189
http://amresearchreview.com/index.php/Journal/about

infections, identifying molecularly imprinted polymers and machine-learning diagnostic models as key emerging tools for pre-diagnostic detection of prosthetic joint infection (PJI), a complication affecting approximately 2% of primary arthroplasties that carries catastrophic clinical consequences when undetected until late-stage presentation. Biosensor-based approaches employing molecularly imprinted polymers (MIPs) have been proposed to selectively capture infection biomarkers, including IL-6, TNF-α, CRP, MMPs, and α-defensin, at the peri-implant surface. Signal transduction via surface-enhanced Raman spectroscopy (SERS) can achieve sub-picomolar analytical sensitivity in purified aqueous buffers, exceeding conventional ELISA performance by more than 100-fold. In complex biofluids such as synovial fluid, SERS sensitivity decreases by approximately 2–3 orders of magnitude versus purified aqueous buffers, shifting the effective detection limit from sub-picomolar to low nanomolar range, which remains above clinically relevant biomarker concentrations (e.g., synovial IL-6 in PJI: typically 10–100 ng/mL). Machine-learning meta-models processing sensor output demonstrate high diagnostic accuracy, substantially outperforming current clinical diagnostic criteria for PJI. The principal translational impediment is biofouling of electrochemical sensor surfaces rather than algorithmic capability, with zwitterionic polymer coatings identified as the primary engineering target for mitigation [9].

7. Translational Challenges and the Regulatory Landscape

7.1 Manufacturing Challenges

The transition from laboratory-scale scaffold prototypes to clinical-grade, GMP-manufactured products constitutes the most formidable non-scientific challenge confronting the BTE field. For cell-laden constructs, terminal sterilisation is categorically incompatible with cell viability, necessitating cleanroom aseptic manufacturing processes with associated costs that remain prohibitive for routine clinical deployment. Bioprinting introduces additional manufacturing challenges, including nozzle occlusion, shear-mediated cell damage during extrusion, and progressive degradation of spatial print accuracy. For integrated diagnostic scaffolds, non-specific protein adsorption (biofouling) onto conductive sensor surfaces constitutes the predominant material engineering challenge, progressively degrading electrochemical sensor performance over weeks to months in the in vivo environment [9,65].

7.2 Regulatory Classification

Advanced BTE scaffolds face demanding regulatory classification pathways. Regulatory classification is risk-stratified and product-specific. Under EU MDR 2017/745 Annex VIII Rule 8: non-resorbable acellular bone scaffolds (as non-resorbable surgical implants) are typically Class IIb; resorbable bone void fillers and resorbable load-bearing bone substitutes are Class III regardless of resorption time, since Rule 8 specifies that all resorbable implantable devices fall into Class III. These classifications follow MDR Annex VIII rules based on duration of contact, absorption behaviour, and anatomical site, and no single blanket class applies across the entire product range [107]. In the United States, acellular bone void fillers may be 510(k)-cleared Class II devices, while permanent, load-bearing, or complex acellular implants may require Class III/PMA pathways depending on intended use, contact duration, and

Annual Methodological Archive Research Review
http://amresearchreview.com/index.php/Journal/about
Volume 4, Issue 2 (2026)

Online ISSN 3007-3197
Print ISSN 3007-3189
http://amresearchreview.com/index.php/Journal/about

material novelty. Scaffolds incorporating living cells or recombinant growth factors are classified as Advanced Therapy Medicinal Products (ATMPs) in Europe, requiring concurrent demonstration of safety, identity, purity, potency, and clinical efficacy, with development timelines of 10–15 years and approval costs typically exceeding EUR 100 million. Integrated biosensor scaffold systems require simultaneous navigation of both ATMP and Software as a Medical Device (SaMD) regulatory pathways, a dual classification framework that is presently unprecedented and urgently requires regulatory resolution [9].

7.3 The Aged Preclinical Model Problem

All major systematic reviews converge on a critical and largely unaddressed systematic bias: the substantial majority of BTE scaffold studies employ young, immunocompetent animal models and young donor cell populations, despite the primary clinical target population consisting predominantly of elderly patients with compromised regenerative biology. [108] Data derived from young-animal models systematically and substantially overestimate scaffold efficacy in aged recipients, because the aged skeletal microenvironment, characterised by chronically elevated ROS, macrophage-mediated inflammaging, reduced endothelial progenitor cell and MSC numbers, and attenuated angiogenic capacity, is biologically distinct from the young healing milieu. Multiple independent research groups have explicitly called for the establishment of an international consortium to develop and adopt consensus protocols for aged skeletal biomaterial evaluation [5,7,16].

8. Future Research Directions

On the basis of synthesis across all reviewed sources, the following research priorities are identified for the next decade of BTE development. The integration of multi-responsive platforms combining pH-buffering, ROS-scavenging, MMP-responsive, immunomodulatory, and senolytic functionalities within a single coordinated scaffold is identified as the most impactful near-term research direction. [109,110,111–112,113,114,115] Standardised aged preclinical model protocols require development and international harmonisation as prerequisites for preclinical data capable of informing clinical translation in elderly patient populations. Vascularisation strategies must progress towards simultaneous recreation of H-type and L-type vascular subtypes within scaffold architectures. Targeted investigation of anti-biofouling material strategies, specifically zwitterionic polymer coatings, is required to extend the functional longevity of integrated diagnostic scaffold systems. Four-dimensional bioprinting and shape-memory scaffold constructs capable of dynamic adaptation to the evolving healing microenvironment represent the principal next fabrication frontier. Machine-learning-guided scaffold design for multi-variable material property prediction and combinatorial composition screening has substantial potential to accelerate the optimisation cycle [5,13,16].

Table 8.1. Priority future research directions for bioactive scaffold development in bone tissue engineering.

Priority Area	Current	Proposed Direction	Key	Evidence

Annual Methodological Archive Research Review
http://amresearchreview.com/index.php/Journal/about
Volume 4, Issue 2 (2026)

Online ISSN 3007-3197
Print ISSN 3007-3189
http://amresearchreview.com/index.php/Journal/about

	Limitation		Source
Multi-responsive platforms	Single-modality systems insufficient for aged bone	Integrated pH-buffering + ROS-scavenging + MMP-responsive + senolytic scaffold	Li 2026; Schwartzman 2024
Aged preclinical models	Young-model data overestimates efficacy in elderly	International consensus protocols; aged donor cell requirements; OVX models	Multiple 2024-2026 reviews
Vascularisation	H-type/L-type vessel recreation unresolved	Spatial co-delivery of subtype-specific angiogenic factors; dual-zone architecture	Fan 2025; Awad 2023
Anti-biofouling for AI scaffolds	Protein adsorption degrades sensor within weeks	Zwitterionic polymer (MPC) coatings; dynamic anti-fouling surfaces	Peel 2024; Lancet Microbe
4D bioprinting	Static geometries cannot adapt to healing microenvironment	Shape-memory scaffolds with programmed deployment; temperature/pH-responsive constructs	Montoya 2021

9. Conclusion

Bioactive scaffolds for bone tissue engineering have undergone a profound conceptual transformation over the preceding two decades, progressing from passive, bioinert structural supports to intelligent, multi-functional platforms that autonomously sense the healing microenvironment, modulate the immune response, deliver therapeutic cargo with spatial and temporal precision, and in their most advanced embodiments, continuously surveil for pre-diagnostic infection signatures.

Five overarching conclusions emerge from this review. First, the global clinical and economic burden of bone defect repair, encompassing approximately 22.3 million orthopaedic procedures annually and costs exceeding US$25 billion in the United States and approximately EUR 28 billion in Europe, establishes a compelling and urgent imperative for more effective bioactive scaffold technologies. Second, compressive strength data across material and fabrication classes confirm that dense sintered HAp (approximately 100–300 MPa) achieves the highest structural performance among bioceramic scaffold materials, while the Ryshkewitch exponential porosity–strength relationship fundamentally constrains all scaffold designs toward composite and architecturally graded solutions. Third, prevascularised constructs incorporating HUVEC–MSC co-culture with sequential VEGF and BMP-2 delivery achieve bone volume fractions approaching 60%, substantially exceeding acellular and single-cell controls, confirming prevascularisation as the most effective currently validated vascularisation strategy.

Fourth, piezoelectric biomaterials, particularly PVDF/$BaTiO_3$ composites (d_{33} approximately 75 pC/N), represent the most advanced autonomous osteogenic and

Online ISSN 3007-3197
Print ISSN 3007-3189

antibacterial stimulation platform, operating without exogenous growth factor supplementation under physiological mechanical loading. Fifth, strategic mapping of scaffold categories by manufacturing complexity and clinical evidence level confirms that the translational trajectory progresses from acellular and polymer scaffolds (mature, well-established) through bioprinted constructs (emerging clinical validation) to smart and biosensor-integrated systems (frontier, high translational potential with significant residual engineering and regulatory challenges).

Looking forward, successful clinical translation of next-generation BTE scaffolds will be contingent upon four prerequisites: the development and international adoption of standardised aged preclinical evaluation models; the establishment of GMP-compatible manufacturing processes for complex multi-functional scaffold constructs; the development of coherent regulatory frameworks adapted to combination ATMP/SaMD classification; and the formation of international pre-competitive consortia to drive harmonised technical and regulatory standards. The fundamental scientific knowledge base is well established. The principal remaining barriers are translational, regulatory, and organisational rather than basic scientific in nature.

Funding Statement

This research did not receive any specific funding from public, commercial, or not-for-profit agencies.

Conflict of Interest

The authors declare no conflict of interest.

Data Availability

The data supporting the findings of this study are available from the corresponding author upon reasonable request.

Author's Contribution

Faizan Azmat (Supervisor): conceptualisation, research design, overall supervision, critical revision of the manuscript, and final approval of the submitted version. Arisha Ijaz: lead author; conducted the primary literature search, synthesised evidence across all four BTE domains, coordinated the manuscript structure, and prepared the final draft. Alishba Gulfam: contributed to the scaffold material classes section, prepared figures and tables, and performed manuscript editing and formatting. Eisha Fatima: responsible for data collection, data analysis, quantitative interpretation of mechanical and biological results, reference management, source verification, and manuscript review. Maryam Hanif: contributed to literature synthesis on vascularisation and smart scaffold strategies, background research on fabrication technologies, table preparation, manuscript proofreading, and final submission preparation.

References

[1] Liu, Y. et al. (2020). Facilitated vascularization and enhanced bone regeneration by manipulation of hierarchical pore structure of scaffolds. Materials Science and Engineering: C, 110, 110622. DOI: 10.1016/j.msec.2019.110622

[2] Schmitz, J.P. & Hollinger, J.O. (1986). The Critical Size Defect as an Experimental Model for Craniomandibulofacial Nonunions. Clinical Orthopaedics and Related Research, 205, 299–308. DOI: 10.1097/00003086-198604000-00036

[3] Wei, J., Chen, X., Xu, Y., Shi, L., Zhang, M., Nie, M. & Liu, X. (2024). Significance

Online ISSN 3007-3197
Print ISSN 3007-3189

and considerations of establishing standardised critical values for critical size defects in animal models of bone tissue regeneration. Heliyon, 10(13), e33768. DOI: 10.1016/j.heliyon.2024.e33768

[4] Winkler, T., Sass, F.A., Duda, G.N. & Schmidt-Bleek, K. (2018). A Review of Biomaterials in Bone Defect Healing, Remaining Shortcomings and Future Opportunities for Bone Tissue Engineering. Bone & Joint Research, 7(3), 232-243. DOI: 10.1302/2046-3758.73.BJR-2017-0270.R1

[5] Liang, D. et al. (2026). Smart Biomaterials for Skeletal Aging Repair and Regeneration. Bone Research (Nature Partner Journal). DOI: 10.1038/s41413-026-00505-9

[6] GBD 2019 Fractures Collaborators (2021). The global, regional, and national burden of fractures in 204 countries and territories, 1990–2019: a systematic analysis from the Global Burden of Disease Study 2019. Lancet Healthy Longevity, 2(9), e580–e592. DOI: 10.1016/S2666-7568(21)00146-0.

[7] Schwartzman, J.D. et al. (2024). Multifunctional Scaffolds for Bone Repair Following Age-Related Biological Decline: Promising Prospects for Smart Biomaterial-Driven Technologies. Biomaterials, 311, 122683. DOI: 10.1016/j.biomaterials.2024.122683

[8] Fan, J., Ding, Z., Cai, Y., Lai, Y., Huang, C., Jiang, B., Zhou, Z. & Luo, Z. (2025). Revolutionizing Bone Regeneration: Vascularized Bone Tissue Engineering with Advanced 3D Printing Technology. Aggregate, 6, e731. DOI: 10.1002/agt2.731

[9] Imam, M.A. et al. (2024). Intersection of artificial intelligence, microbes, and bone and joint infections: a new frontier for improving management outcomes. The Lancet Microbe, 6(3), 101008. DOI: 10.1016/j.lanmic.2024.101008

[10] Turnbull, G. et al. (2018). 3D Bioactive Composite Scaffolds for Bone Tissue Engineering. Bioactive Materials, 3(3), 278-314. DOI: 10.1016/j.bioactmat.2017.10.001

[11] De Pace, R., Iaquinta, M.R., Benkhalqui, A., D'Agostino, A., Trevisiol, L., Nocini, R., Mazziotta, C., Rotondo, J.C., Bononi, I., Tognon, M., Martini, F. & Mazzoni, E. (2025). Revolutionizing bone healing: the role of 3D models. Cell Regeneration, 14, 7. DOI: 10.1186/s13619-025-00225-1

[12] Deplaigne, V. & Rochefort, G.Y. (2022). Bone tissue engineering at a glance. AIMS Bioengineering, 9(1), 22-25. DOI: 10.3934/bioeng.2022002

[13] Montoya, C. et al. (2021). On the Road to Smart Biomaterials for Bone Research: Definitions, Concepts, Advances, and Outlook. Bone Research (Nature Partner Journal), 9, 12. DOI: 10.1038/s41413-020-00131-z

[14] Liang, W. et al. (2024). Nanotechnology-based bone regeneration in orthopedics: A review of recent trends. Nanomedicine: Nanotechnology, Biology and Medicine, 19(3), 255-275. DOI: 10.2217/nnm-2023-0187

[15] Liang, W., Zhou, C., Bai, J., Zhang, H., Jiang, B., Wang, J., Fu, L., Long, H., Huang, X., Zhao, J. & Zhu, H. (2024). Current advancements in therapeutic approaches in orthopedic surgery: a review of recent trends. Frontiers in Bioengineering and Biotechnology, 12. DOI: 10.3389/fbioe.2024.1328997

[16] Sun, T. et al. (2025). Bone Tissue Engineering Scaffolds for Bone Aging: Drug Delivery and Microenvironment Regulation. Tissue Engineering Part B:

Online ISSN 3007-3197
Print ISSN 3007-3189

Reviews. OnlineFirst, 26 September 2025. DOI: 10.1177/19373341251379774

[17] Bolamperti, S., Villa, I. & Rubinacci, A. (2022). Bone Remodeling: An Operational Process Ensuring Survival and Bone Mechanical Competence. Bone Research, 10(1), 48. DOI: 10.1038/s41413-022-00219-8

[18] Rho, J.Y., Kuhn-Spearing, L. & Zioupos, P. (1998). Mechanical Properties and the Hierarchical Structure of Bone. Medical Engineering & Physics, 20(2), 92–102. DOI: 10.1016/S1350-4533(98)00007-1

[19] Mondal, S. et al. (2023). Hydroxyapatite: A Journey from Biomaterials to Advanced Functional Materials. Advances in Colloid and Interface Science, 321, 103013. DOI: 10.1016/j.cis.2023.103013

[20] Millán, J.L. (2006). Alkaline Phosphatases: Structure, substrate specificity and functional related aspects to mammalian and lower eukaryote. Wiley-VCH, Weinheim. [Reference for ALP isoenzyme classification.]

[21] Ma, Q., Miri, Z., Haugen, H.J., Moghanian, A. & Loca, D. (2023). Significance of mechanical loading in bone fracture healing, bone regeneration, and vascularization. Journal of Tissue Engineering, 14, 20417314231172573. DOI: 10.1177/20417314231172573

[22] Zha, K. et al. (2022). Recent Advances in Enhancement Strategies for Osteogenic Differentiation of Mesenchymal Stem Cells in Bone Tissue Engineering. Frontiers in Cell and Developmental Biology, 10, 824812. DOI: 10.3389/fcell.2022.824812

[23] Bai, X. et al. (2023). Dental Pulp Stem Cells for Bone Tissue Engineering: A Literature Review. Stem Cells International, 2023, 7357179. DOI: 10.1155/2023/7357179

[24] Meesuk, L., Suwanprateeb, J., Thammarakcharoen, F., Tantrawatpan, C., Kheolamai, P., Palang, I., Tantikanlayaporn, D. & Manochantr, S. (2022). Osteogenic differentiation and proliferation potentials of human bone marrow and umbilical cord-derived mesenchymal stem cells on the 3D-printed hydroxyapatite scaffolds. Scientific Reports, 12, 19509. DOI: 10.1038/s41598-022-24160-2

[25] Engler, A.J., Sen, S., Sweeney, H.L. & Discher, D.E. (2006). Matrix Elasticity Directs Stem Cell Lineage Specification. Cell, 126(4), 677-689. DOI: 10.1016/j.cell.2006.06.044

[26] Bhushan, S., Singh, S., Maiti, T.K., Sharma, C., Dutt, D., Sharma, S., Li, C. & Tag Eldin, E.M. (2022). Scaffold Fabrication Techniques of Biomaterials for Bone Tissue Engineering: A Critical Review. Bioengineering, 9(12), 728. DOI: 10.3390/bioengineering9120728

[27] Chen, S. et al. (2023). Piezocatalytic Medicine: An Emerging Frontier using Piezoelectric Materials for Biomedical Applications. Advanced Materials, 35(25), 2208256. DOI: 10.1002/adma.202208256

[28] Abere, D.V. et al. (2022). Mechanical and morphological characterization of nano-hydroxyapatite (nHA) for bone regeneration: A mini review. Biomedical Engineering Advances, 4, 100056. DOI: 10.1016/j.bea.2022.100056

[29] Gerhardt, L.C. & Boccaccini, A.R. (2010). Bioactive Glass and Glass-Ceramic Scaffolds for Bone Tissue Engineering. Materials, 3(7), 3867-3910. DOI:

Online ISSN 3007-3197
Print ISSN 3007-3189

10.3390/ma3073867

[30] Hench, L.L. (2006). The story of Bioglass. Journal of Materials Science: Materials in Medicine, 17(11), 967–978. DOI: 10.1007/s10856-006-0432-z. [Cross-referenced to ref [41] to substantiate dense Bioglass 45S5 mechanical property.]

[31] Bohner, M. (2010). Resorbable Biomaterials as Bone Graft Substitutes. Materials Today, 13(1–2), 24–30. DOI: 10.1016/S1369-7021(10)70014-6

[32] Bohner, M. (2010). Resorbable Biomaterials as Bone Graft Substitutes. Materials Today, 13(1–2), 24–30. DOI: 10.1016/S1369-7021(10)70014-6. [Cross-referenced to ref [31] to substantiate the osteoconductive-versus-osteoinductive distinction for calcium phosphate ceramics.]

[33] Amiryaghoubi, N. & Jahanban Esfahlan, R. (2024). Applications of Hydroxyapatite-Based Polymeric Scaffolds in Bone Tissue Engineering: An Update. Advanced Pharmaceutical Bulletin, 14(4), 794-806. DOI: 10.34172/apb.43818

[34] Du, M. et al. (2021). Recent advances in biomedical engineering of nano-hydroxyapatite including dentistry, cancer treatment and bone repair. Composites Part B: Engineering, 215, 108790. DOI: 10.1016/j.compositesb.2021.108790

[35] Bianchi, E. et al. (2022). Inorganic Nanomaterials in Tissue Engineering. Pharmaceutics, 14(6), 1127. DOI: 10.3390/pharmaceutics14061127

[36] Radha, G., Manjubaashini, N. & Balakumar, S. (2023). Nano-hydroxyapatite/natural polymer composite scaffolds for bone tissue engineering: a brief review of recent trend. In Vitro Models, 2(5), 125-151. DOI: 10.1007/s44164-023-00049-w

[37] Mysore, T.H.M. et al. (2024). Apatite insights: From synthesis to biomedical applications. European Polymer Journal, 209, 112842. DOI: 10.1016/j.eurpolymj.2024.112842

[38] Liu, W. et al. (2025). Application of Hydroxyapatite Composites in Bone Tissue Engineering: A Review. Journal of Functional Biomaterials, 16(4), 127. DOI: 10.3390/jfb16040127

[39] Nogueira, D.M.B. et al. (2024). Update on the use of 45S5 bioactive glass in the treatment of bone defects in regenerative medicine. World Journal of Orthopedics, 15(3), 204-214. DOI: 10.5312/wjo.v15.i3.204

[40] Jin, Z., Neuville, D.R. & Brauer, D.S. (2025). Glasses for bone regeneration: structural features controlling physical properties and ion release of bioactive glasses 45S5, S53P4 and 13-93. RSC Advances, 15(7), 4997-5006. DOI: 10.1039/d4ra06081d

[41] Hench, L.L. (2006). The story of Bioglass. Journal of Materials Science: Materials in Medicine, 17(11), 967-978. DOI: 10.1007/s10856-006-0432-z

[42] Pittet, C.O., Freitas, R.M., Bow, J.R. & Boccaccini, A.R. (2023). Bioactive glass scaffolds for bone tissue engineering: a review. Journal of the European Ceramic Society, 43(5), 2117–2135. DOI: 10.1016/j.jeurceramsoc.2022.12.040.

[43] Li, M. et al. (2023). A Comprehensive Review on Silk Fibroin as a Persuasive Biomaterial for Bone Tissue Engineering. International Journal of Molecular Sciences, 24(3), 2660. DOI: 10.3390/ijms24032660

[44] Zhou, B. et al. (2023). GelMA-based bioactive hydrogel scaffolds with multiple

Online ISSN 3007-3197
Print ISSN 3007-3189

bone defect repair functions: therapeutic strategies and recent advances. Biomaterials Research, 27, 86. DOI: 10.1186/s40824-023-00422-6

[45] Walejewska, E. et al. (2024). Tuning Physical Properties of GelMA Hydrogels through Microarchitecture for Engineering Osteoid Tissue. Biomacromolecules, 25(1), 188-199. DOI: 10.1021/acs.biomac.3c00909

[46] Collins, M.N. et al. (2021). Scaffold Fabrication Technologies and Structure/Function Properties in Bone Tissue Engineering. Advanced Functional Materials, 31(21), 2010609. DOI: 10.1002/adfm.202010609

[47] Lacambra-Andreu, X. et al. (2023). A Review on Manufacturing Processes of Biocomposites Based on Poly(alpha-Esters) and Bioactive Glass Fillers for Bone Regeneration. Biomimetics, 8(1), 81. DOI: 10.3390/biomimetics8010081

[48] Woodruff, M.A. & Hutmacher, D.W. (2010). The Return of a Forgotten Polymer: Polycaprolactone in the 21st Century. Progress in Polymer Science, 35(10), 1217–1256. DOI: 10.1016/j.progpolymsci.2010.04.002

[49] Mo, X. et al. (2023). Nano-Hydroxyapatite Composite Scaffolds Loaded with Bioactive Factors and Drugs for Bone Tissue Engineering. International Journal of Molecular Sciences, 24(2), 1291. DOI: 10.3390/ijms24021291

[50] Chen, Z. et al. (2024). Advanced Hybrid Strategies of GelMA Composite Hydrogels in Bone Defect Repair. Polymers, 16(21), 3039. DOI: 10.3390/polym16213039

[51] Ma, P. et al. (2021). Biomimetic gelatin/chitosan/polyvinyl alcohol/nano-hydroxyapatite scaffolds for bone tissue engineering. Materials & Design, 207, 109865. DOI: 10.1016/j.matdes.2021.109865

[52] Jin, S. et al. (2023). Chopped fibers and nano-hydroxyapatite enhanced silk fibroin porous hybrid scaffolds for bone augmentation. Journal of Materials Chemistry B, 11(7), 1557-1567. DOI: 10.1039/d2tb02510h

[53] Sun, S. et al. (2023). Drug delivery systems based on polyethylene glycol hydrogels for enhanced bone regeneration. Frontiers in Bioengineering and Biotechnology, 11, 1117647. DOI: 10.3389/fbioe.2023.1117647

[54] Yoon, S.J. et al. (2023). Accelerating bone regeneration using poly(lactic-co-glycolic acid)/hydroxyapatite scaffolds containing duck feet-derived collagen. International Journal of Biological Macromolecules, 229, 486-495. DOI: 10.1016/j.ijbiomac.2022.12.296

[55] Li, M. et al. (2024). Improved biocompatibility and osteogenesis of porous graphene oxide/silk fibroin scaffold for bone tissue engineering applications. Materials Today Communications, 40, 109480. DOI: 10.1016/j.mtcomm.2024.109480

[56] Wang, Y. et al. (2020). A GelMA-PEGDA-nHA Composite Hydrogel for Bone Tissue Engineering. Materials, 13(17), 3735. DOI: 10.3390/ma13173735

[57] Nulty, J. et al. (2021). 3D Bioprinting of Prevascularised Implants for the Repair of Critically-Sized Bone Defects. Acta Biomaterialia, 126, 154-169. DOI: 10.1016/j.actbio.2021.03.003

[58] Garot, C. et al. (2023). 3D-Printed Osteoinductive Polymeric Scaffolds with Optimized Architecture to Repair a Sheep Metatarsal Critical-Size Bone Defect. Advanced Healthcare Materials, 12(30), e2301692. DOI:

Online ISSN 3007-3197
Print ISSN 3007-3189

10.1002/adhm.202301692

[59] Soleymani, S. & Naghib, S.M. (2023). 3D and 4D printing hydroxyapatite-based scaffolds for bone tissue engineering and regeneration. Heliyon, 9(9), e19363. DOI: 10.1016/j.heliyon.2023.e19363

[60] Palivela, B.C. et al. (2022). Extrusion-based 3D printing of bioactive glass scaffolds: process parameters and mechanical properties: a review. Bioprinting, 27, e00219. DOI: 10.1016/j.bprint.2022.e00219

[61] Liu, K. et al. (2025). 3D-printed porous calcium silicate scaffolds with hydroxyapatite/graphene oxide hybrid coating for guided bone regeneration. Ceramics International, 51(1), 1103-1114. DOI: 10.1016/j.ceramint.2024.11.092

[62] Babaei, M. et al. (2024). A comprehensive bench-to-bed evaluation of 3D-printed polycaprolactone/hydroxyapatite implants for craniomaxillofacial defects. Biomaterials Advances, 161, 213900. DOI: 10.1016/j.bioadv.2024.213900

[63] Ebrahimi, Z. et al. (2022). Enhanced osteogenic differentiation of stem cells by 3D printed PCL scaffolds coated with collagen and hydroxyapatite. Scientific Reports, 12, 12069. DOI: 10.1038/s41598-022-15602-y

[64] Hsieh, F.Y., Tao, H.Y., Lin, Y.C. & Hsu, S.H. (2022). Fabrication of cell-laden GelMA scaffolds by two-photon polymerisation. Biofabrication, 14(3), 035010. DOI: 10.1088/1758-5090/ac6c7f.

[65] Sagar, N., Chakravarti, B., Maurya, S.S., Nigam, A., Malakar, P. & Kashyap, R. (2024). Unleashing innovation: 3D-printed biomaterials in bone tissue engineering for repairing femur and tibial defects in animal models — a systematic review and meta-analysis. Frontiers in Bioengineering and Biotechnology, 12, 1385365. DOI: 10.3389/fbioe.2024.1385365

[66] Ryshkewitch, E. (1953). Compression Strength of Porous Sintered Alumina and Zirconia. Journal of the American Ceramic Society, 36(2), 65–68. DOI: 10.1111/j.1151-2916.1953.tb12837.x

[67] Martin, R.I. & Brown, P.W. (1995). Mechanical properties of hydroxyapatite formed at physiological temperature. Journal of Materials Science: Materials in Medicine, 6(3), 138–143. DOI: 10.1007/BF00120207. [HAp-specific application of the Ryshkewitch porosity–strength relationship.]

[68] Karageorgiou, V. & Kaplan, D. (2005). Porosity of 3D Biomaterial Scaffolds and Osteogenesis. Biomaterials, 26(27), 5474-5491. DOI: 10.1016/j.biomaterials.2005.02.002

[69] Hayashi, K. et al. (2022). Effects of scaffold shape on bone regeneration: tiny shape differences affect the entire system. ACS Nano, 16(8), 11755-11768. DOI: 10.1021/acsnano.2c03776

[70] Hollister, S.J. (2005). Porous Scaffold Design for Tissue Engineering. Nature Materials, 4(7), 518-524. DOI: 10.1038/nmat1421

[71] Elkhouly, H., Mamdouh, W. & El-Korashy, D.I. (2021). Electrospun nano-fibrous bilayer scaffold prepared from polycaprolactone/gelatin and bioactive glass for bone tissue engineering. Journal of Materials Science: Materials in Medicine, 32, 108. DOI: 10.1007/s10856-021-06588-6

[72] Rahmati, M. et al. (2021). Electrospinning for tissue engineering applications. Progress in Materials Science, 117, 100721. DOI:

Online ISSN 3007-3197
Print ISSN 3007-3189

10.1016/j.pmatsci.2020.100721

[73] Mohammadalizadeh, Z. et al. (2022). Synthetic-based blended electrospun scaffolds in tissue engineering applications. Journal of Materials Science, 57, 4020-4079. DOI: 10.1007/s10853-021-06826-w

[74] Zhou, C. et al. (2022). Engineered electrospun poly(lactic-co-glycolic acid)/Si3N4 nanofiber scaffold promotes osteogenesis of mesenchymal stem cells. Frontiers in Materials, 9, 991018. DOI: 10.3389/fmats.2022.991018

[75] Guzman-Soria, A. et al. (2023). Effect of electrospun PLGA/collagen scaffolds on cell adhesion, viability, and collagen release: potential applications in tissue engineering. Polymers, 15(5), 1079. DOI: 10.3390/polym15051079

[76] Zhang, Y. et al. (2024). Stepwise degradable PGA-SF core-shell electrospinning scaffold for bone regeneration. Materials Today Bio, 26, 101023. DOI: 10.1016/j.mtbio.2024.101023

[77] Weiner, S. & Wagner, H.D. (1998). The Material Bone: Structure-Mechanical Function Relations. Annual Review of Materials Science, 28, 271–298. DOI: 10.1146/annurev.matsci.28.1.271

[78] Awad, K., Ahuja, N., Yacoub, A.S., Brotto, L., Young, S., Mikos, A., Aswath, P. & Varanasi, V. (2023). Revolutionizing bone regeneration: advanced biomaterials for healing compromised bone defects. Frontiers in Aging, 4, 1217054. DOI: 10.3389/fragi.2023.1217054

[79] Lv, N. et al. (2023). Research progress of vascularization strategies of tissue-engineered bone. Frontiers in Bioengineering and Biotechnology, 11, 1291969. DOI: 10.3389/fbioe.2023.1291969

[80] Shakeel, A. & Corridon, P.R. (2023). Mitigating challenges and expanding the future of vascular tissue engineering — are we there yet? Frontiers in Physiology, 13, 1079421. DOI: 10.3389/fphys.2022.1079421

[81] Ellermann, E. et al. (2023). In vitro angiogenesis in response to biomaterial properties for bone tissue engineering: a review of the state of the art. Regenerative Biomaterials, 10, rbad027. DOI: 10.1093/rb/rbad027

[82] Zare Jalise, S. et al. (2026). Advancements in Promoting Angiogenesis in Tissue-Engineered Grafts in Various Organs: A Comprehensive Review. Macromolecular Bioscience, 26(3), e202500453. DOI: 10.1002/mabi.202500453

[83] Carmeliet, P. & Jain, R.K. (2000). Angiogenesis in Cancer and Other Diseases. Nature, 407(6801), 249–257. DOI: 10.1038/35025220

[84] Pobloth, A.M. et al. (2018). Mechanobiologically optimized 3D titanium-mesh scaffolds enhance bone regeneration in critical segmental defects in sheep. Science Translational Medicine, 10(423), eaam8828. DOI: 10.1126/scitranslmed.aam8828

[85] Ren, B. et al. (2022). Osteogenic Differentiation of Human Adipose-Derived Stem Cells Seeded on a Biomimetic Spongiosa-like Scaffold: BMP-2 Delivery by Overexpressing Fascia. International Journal of Molecular Sciences, 23(5), 2712. DOI: 10.3390/ijms23052712

[86] Yang, X. et al. (2022). BMP-2 promotes osteogenic differentiation of mesenchymal stem cells by enhancing mitochondrial activity. Journal of Musculoskeletal and Neuronal Interactions, 22(1), 123-131. PMID: 35234167.

Online ISSN 3007-3197
Print ISSN 3007-3189

PMCID: PMC8919656

[87] Pizzicannella, J. et al. (2023). Addendum: Engineered extracellular vesicles from human periodontal-ligament stem cells increase VEGF/VEGFR2 expression during bone regeneration. Frontiers in Physiology, 14, 1148929. DOI: 10.3389/fphys.2023.1148929

[88] Xue, X. et al. (2021). Recent Advances in Design of Functional Biocompatible Hydrogels for Bone Tissue Engineering. Advanced Functional Materials, 31(19), 2009432. DOI: 10.1002/adfm.202009432

[89] Hu, W. et al. (2024). Engineered exosomes and composite biomaterials for tissue regeneration. Theranostics, 14(5), 2099-2126. DOI: 10.7150/thno.93088

[90] Yu, T. et al. (2024). Extracellular vesicle-functionalized bioactive scaffolds for bone regeneration. Asian Journal of Pharmaceutical Sciences, 19(5), 100945. DOI: 10.1016/j.ajps.2024.100945

[91] Deng, H., Wang, J. & An, R. (2023). Hyaluronic acid-based hydrogels as an exosome delivery system in bone regeneration. Frontiers in Pharmacology, 14, 1131001. DOI: 10.3390/fphar.2023.1131001

[92] Chen, L. et al. (2022). Multifunctional hydrogel enhances bone regeneration through sustained release of stromal cell-derived factor-1alpha and exosomes. Bioactive Materials, 25, 460-471. DOI: 10.1016/j.bioactmat.2022.07.030

[93] Hwang, H.S. & Lee, C.-S. (2024). Exosome-integrated hydrogels for bone tissue engineering. Gels, 10(12), 762. DOI: 10.3390/gels10120762

[94] Wang, L. et al. (2025). Exosome-capturing scaffold promotes endogenous bone regeneration through neutrophil-derived exosomes by enhancing fast vascularization. Biomaterials, 319, 123215. DOI: 10.1016/j.biomaterials.2025.123215

[95] Sun, T. et al. (2024). Novel 3D-printing bilayer GelMA-based hydrogel containing BP, beta-TCP and exosomes for cartilage-bone integrated repair. Biofabrication, 16(1), 015008. DOI: 10.1088/1758-5090/ad04fe

[96] Wang, D. et al. (2024). Cell membrane vesicles derived from hBMSCs and hUVECs enhance bone regeneration. Bone Research, 12, 23. DOI: 10.1038/s41413-024-00325-9

[97] Wang, Z. et al. (2025). 4D printing polymeric biomaterials for adaptive tissue regeneration. Bioactive Materials, 48, 370-399. DOI: 10.1016/j.bioactmat.2025.01.033

[98] Yuan, X., Zhu, W., Yang, Z., He, N., Chen, F., Han, X. & Zhou, K. (2024). Recent Advances in 3D Printing of Smart Scaffolds for Bone Tissue Engineering and Regeneration. Advanced Materials, 36(34), 2403641. DOI: 10.1002/adma.202403641

[99] Percival, K.M., Paul, V. & Husseini, G.A. (2024). Recent Advancements in Bone Tissue Engineering: Integrating Smart Scaffold Technologies and Bio-Responsive Systems for Enhanced Regeneration. International Journal of Molecular Sciences, 25(11), 6012. DOI: 10.3390/ijms25116012

[100] Lee, P.S. et al. (2022). The interplay of collagen/bioactive glass nanoparticle coatings and electrical stimulation regimes distinctly enhanced osteogenic differentiation of human mesenchymal stem cells. Acta Biomaterialia, 149, 373-

Online ISSN 3007-3197
Print ISSN 3007-3189
http://amresearchreview.com/index.php/Journal/about

386. DOI: 10.1016/j.actbio.2022.06.045
[101] Mirzaei, A. et al. (2019). Synergistic effects of polyaniline and pulsed electromagnetic field to stem cells osteogenic differentiation on polyvinylidene fluoride scaffold. Artificial Cells, Nanomedicine and Biotechnology, 47(1), 3058-3066. DOI: 10.1080/21691401.2019.1645154
[102] Zaszczyńska, A. et al. (2024). Piezoelectric Scaffolds as Smart Materials for Bone Tissue Engineering. Polymers, 16(19), 2797. DOI: 10.3390/polym16192797
[103] Amiri, E., Khakbiz, M., Bakhshandeh, B., Ranjbar, N. & Mohammadnejad, J. (2024). Enhancing osteogenic differentiation of mesenchymal stem cells seeded on a polycaprolactone/MoS2 nanofibrous scaffold through electrical stimulation. Molecular Systems Design & Engineering, 9, 581–596. DOI: 10.1039/D3ME00135K
[104] Dong, Y., Suryani, L., Zhou, X., Muthukumaran, P., Rakshit, M., Yang, F., Wen, F., Hassanbhai, A.M., Parida, K., Simon, D.T., Iandolo, D., Lee, P.S., Ng, K.W. & Teoh, S.H. (2021). Synergistic Effect of PVDF-Coated PCL-TCP Scaffolds and Pulsed Electromagnetic Field on Osteogenesis. International Journal of Molecular Sciences, 22(12), 6438. DOI: 10.3390/ijms22126438
[105] Huang, H., Wang, K., Liu, X., Liu, X., Wang, J., Suo, M., Wang, H., Chen, S., Chen, X. & Li, Z. (2025). Piezoelectric biomaterials for providing electrical stimulation in bone tissue engineering: Barium titanate. Journal of Orthopaedic Translation, 51, 94–107. DOI: 10.1016/j.jot.2024.12.011
[106] Kazimierczak, P. & Przekora, A. (2022). Bioengineered Living Bone Grafts: A Concise Review on Bioreactors and Production Techniques In Vitro. International Journal of Molecular Sciences, 23(3), 1765. DOI: 10.3390/ijms23031765
[107] European Union (2017). Regulation (EU) 2017/745 of the European Parliament and of the Council on medical devices. Official Journal of the European Union, L117, 1–175. [Cited for MDR Annex VIII Rule 8 classification rules.]
[108] Hatt, L.P. et al. (2022). Clinically relevant preclinical animal models for testing novel cranio-maxillofacial bone 3D-printed biomaterials. Clinical and Translational Medicine, 12(2), e690. DOI: 10.1002/ctm2.690
[109] Li, Z. et al. (2023). Biological Scaffolds Assembled with Magnetic Nanoparticles for Bone Tissue Engineering: A Review. Materials, 16(4), 1429. DOI: 10.3390/ma16041429
[110] Rajzer, I. et al. (2025). Four-Dimensional Printing of beta-Tricalcium Phosphate-Modified Shape Memory Polymers for Bone Scaffolds in Osteochondral Regeneration. Materials, 18(2), 306. DOI: 10.3390/ma18020306
[111] Dasari, A., Xue, J. & Deb, S. (2022). Magnetic Nanoparticles in Bone Tissue Engineering. Nanomaterials, 12(5), 757. DOI: 10.3390/nano12050757
[112] Kao, C.-Y. et al. (2022). Synergistic Effect of Static Magnetic Fields and 3D-Printed Iron Oxide Nanoparticle-Containing Calcium Silicate/Poly-epsilon-Caprolactone Scaffolds for Bone Tissue Engineering. Cells, 11(24), 3967. DOI: 10.3390/cells11243967
[113] Cinar Sansegundo, M. et al. (2025). Magnetized Cell-Scaffold Constructs for Bone Tissue Engineering: Advances in Fabrication and Magnetic Stimulation.

Online ISSN 3007-3197
Print ISSN 3007-3189

Advanced Science. DOI: 10.1002/advs.202510094

[114] Yang, J. et al. (2022). Iron oxide nanoparticles combined with static magnetic fields in bone remodeling. Cells, 11(20), 3298. DOI: 10.3390/cells11203298

[115] Wang, N., Xie, Y., Xi, Z., Mi, Z., Deng, R., Liu, X., Kang, H. & Liu, J. (2022). Hope for bone regeneration: The versatility of iron oxide nanoparticles. Frontiers in Bioengineering and Biotechnology, 10, 937803. DOI: 10.3389/fbioe.2022.937803